Phospholipase D Activity Is Regulated by Product Segregation and the Structure Formation of Phosphatidic Acid within Model Membranes

Kerstin Wagner and Gerald Brezesinski
Max Planck Institute of Colloids and Interfaces, 14424 Potsdam, Germany

ABSTRACT Phospholipase D from *Streptomyces chromofuscus* (scPLD) hydrolyzes phosphatidylcholines (PC) to produce choline and phosphatidic acid (PA), a lipid messenger molecule within biological membranes. To scrutinize the influence of membrane structure on scPLD activity, three different substrate-containing monolayers are used as model systems: pure dipalmitoylphosphatidylcholine (DPPC) as well as equimolar mixtures of DPPC/*n*-hexadecanol ($C_{16}OH$) and DPPC/dipalmitoylglycerol (DPG). The activity of scPLD toward these monolayers is tested by infrared reflection-absorption spectroscopy and exhibits different dependencies on surface pressure. For pure DPPC, the catalytic turnover drastically drops above 20 mN/m. On addition of $C_{16}OH$, this strong decrease starts at 5 mN/m. For the DPPC/DPG system, the reaction yield linearly decreases between 5 and 25 mN/m. The difference in scPLD activity is correlated to the phase state of the monolayers as examined by x-ray diffraction, Brewster angle microscopy, and atomic force microscopy. Because the additives $C_{16}OH$ and DPG mediate the miscibility of PC and PA, only a basal activity of scPLD is observed toward the mixed systems at higher surface pressures. At pure DPPC monolayers, scPLD is activated after the segregation of initially formed PA. Furthermore, scPLD is inhibited when the lipids in the PA-rich domains adopt an upright orientation. This phenomenon offers a self-regulating mechanism for the concentration of the second messenger PA within biological membranes.

INTRODUCTION

Phospholipase D (PLD) is an abundant enzyme that hydrolyzes the phosphodiester bond of the predominant membrane phospholipid phosphatidylcholine (PC) to generate phosphatidic acid (PA) and free choline. While the liberated headgroup diffuses away from the interface, PA remains in the membrane and plays different roles as a signaling molecule. Hence, PLD is involved in a variety of cellular processes including lipid metabolism, vesicle trafficking, and signal transduction (1–3).

The PLD from *Streptomyces chromofuscus* (scPLD) is often used to study the enzymatic behavior of PLDs, even though this particular enzyme is not a member of the HKD-phospholipase D superfamily because it does not exhibit the classical sequence motif HKD (4). Instead, so-called non-HKD-PLDs are generally characterized by a dependence on divalent cations and a poor catalysis of the transphosphatidylation reaction (5). In the case of scPLD, a secreted ~57-kDa protein (6), the enzymatic activity depends on the presence of Ca^{2+}. The effect of the ion is associated with promoting scPLD binding to lipid interfaces and/or enhancing the catalytic reaction (7). Accordingly, two functionally distinct phospholipid binding sites are identified: an active site for catalysis (8) and an allosteric binding site, which is specific for PA or other amphiphilic phosphomonoesters (6,9,10). This corroborates the observation that PA is a lipidic activator of scPLD (9). Hence, the generation of a critical amount of PA is related to the end of a lag phase that is part of the typical lag-burst behavior of scPLD (11). It is suggested that a lateral separation of PA induced by Ca^{2+} activates the enzyme (9,11,12). However, a direct proof of the dependence of scPLD on PA segregation is missing.

In this article, we examine the influence of membrane structure on the activity of scPLD. For this purpose, Langmuir monolayers are a highly suitable model that facilitate a distinct manipulation of different parameters including the packing density and phase state of phospholipids. The addition of amphiphilic molecules such as a long-chain alcohol or glycerolipid to a substrate-containing monolayer influences the structure of the system. In this study, we applied monolayers of pure substrate, i.e., DPPC (dipalmitoylphosphatidylcholine), and equimolar mixtures of DPPC/*n*-hexadecanol ($C_{16}OH$) and DPPC/dipalmitoylglycerol (DPG). The three systems provide different initial structures that are assumed to influence the degree of scPLD activity (13). To correlate the enzymatic activity with the model membrane structure, further effects caused by the addition of another amphiphilic molecule to DPPC monolayers must be a priori excluded and are discussed hereafter.

Work by Geng et al. (6,9) shows that scPLD does not prefer micellar versus monomeric substrate and is therefore not interfacially activated as are other enzymes, e.g., phospholipase A_2. Additionally, the enzyme is not sensitive to surface dilution (7). Thus, a dilution of the substrate monolayer on addition of $C_{16}OH$ or DPG does not hinder the catalytic activity of scPLD. In fact, the enzyme is hypothesized to act in a ''hopping'' mode characterized by a nonprocessive catalysis in the presence of an interface (7).

Submitted March 14, 2007, and accepted for publication June 5, 2007.

Address reprint requests to Kerstin Wagner, Max Planck Institute of Colloids and Interfaces, 14424 Potsdam, Germany. Tel.: 49-331-5679212; Fax: 49-331-5679202; E-mail: wagner@mpikg.mpg.de.

Editor: Thomas J. McIntosh.

© 2007 by the Biophysical Society
0006-3495/07/10/2373/11 $2.00

doi: 10.1529/biophysj.107.108787

Furthermore, it is possible that a transphosphatidylation reaction (transP) occurs after addition of an alcohol to the lipid system. During transP, the free hydroxyl group of $C_{16}OH$ or DPG could be used as a nucleophile instead of water. However, we assume that the transP product does not interfere with our study for the following reasons: A study of mixed monolayers of dimyristoylphosphatidylcholine (DMPC) and dimyristoylglycerol (DMG) revealed that the transP product does not accumulate in the monolayer (14). It is immediately hydrolyzed by scPLD to give dimyristoylphosphatidic acid (DMPA) and DMG. The hydrolysis of the transP intermediate is independent of the surface pressure in the monolayer. In addition, hydrolysis and transP exhibit different pH profiles, and the transferase activity of non-HKD-PLDs is much less than their hydrolase activity (5,7).

Here, we test the activity of scPLD toward the three different DPPC-containing systems by infrared reflection-absorption spectroscopy (IRRAS) after establishing a reference system for the quantitative analysis of the reaction yield. The phase state of the substrate-comprising monolayer is determined by x-ray diffraction, Brewster angle microscopy (BAM), and atomic force microscopy (AFM) and then correlated to scPLD activation. The structure formation of domains dominated by the reaction product dipalmitoylphosphatidic acid (DPPA) is shown to affect the inhibition of scPLD.

EXPERIMENTAL PROCEDURES

Material

1,2-Dipalmitoyl-*sn*-glycero-3-phosphocholine, 1,2-dipalmitoyl-*sn*-glycero-3-phosphate (monosodium salt), 1,2-dipalmitoyl-*sn*-glycerol (all from Avanti Polar Lipids, Alabaster, AL), and *n*-hexadecanol (synthesized in house) were used as received and dissolved in chloroform (J T Baker, Deventer, Holland) to give 1 mM stock solutions. These solutions were utilized to prepare mixtures of DPPC/DPPA with different molar mixing ratios. Pure DPPC or DPPC/DPPA solutions were mixed with $C_{16}OH$ or DPG, yielding a molar fraction of the nonphospholipid of 0.5.

PLD from *Streptomyces chromofuscus* was purchased form Sigma-Aldrich (Steinheim, Germany) and used without further purification. Aliquots of the enzyme dissolved in buffer were prepared and stored at −20°C until their application. The aqueous buffer solution consisted of 10 mM Tris (Sigma-Aldrich), 150 mM NaCl (Merck, Darmstadt, Germany), and 120 μM $CaCl_2$ (Sigma-Aldrich) and was adjusted to pH 8.0 with 1 N HCl (Merck). This buffer provides optimal conditions for scPLD (11,14). Water was purified with a Millipore system to give a resistivity of 18.2 MΩ cm.

Langmuir film balance

The surface pressure/area (π/A) isotherms were recorded on a film balance from R&K (Potsdam, Germany), which was equipped with a Wilhelmy-type pressure-measuring system using a filter paper as plate. After the phospholipid-containing solution had been spread on the aqueous buffered subphase, chloroform was allowed to evaporate for 10 min. The monolayer was subsequently compressed at a velocity of 4 Å^2/molecule/min while the π/A isotherm was continuously recorded (cf. Wagner and Brezesinski (13) for compression isotherms). At a surface pressure of 40 mN/m, a first IRRA control spectrum was measured. Subsequently, the enzyme solution (50 units) was injected into the subphase and carefully stirred underneath the monolayer. At 40 mN/m, hydrolysis could not be observed. The monolayer was then expanded to a defined surface pressure, at which the hydrolytic process was detected by IRRA spectroscopy. Two automatically moving barriers kept the surface pressure constant during the reaction process. After its completion, the monolayer was again compressed to 40 mN/m, and a final IRRA control spectrum was recorded. Each experiment was repeated at least two times. The temperature T was maintained at 20°C during all experiments described in this article.

IRRA spectroscopy

Spectra were acquired with an IFS 66 FT-IR spectrometer from Bruker (Ettlingen, Germany) equipped with an external reflectance unit containing a Langmuir trough setup. The infrared beam is directed through the external port of the spectrometer and is subsequently reflected by three mirrors in a rigid mount before being focused on the water surface. A KRS-5 wire grid polarizer is placed in the optical path directly before the beam hits the water surface. The reflected light is collected at the same angle as the angle of incidence. The light then follows an equivalent mirror path and is directed onto a narrow-band mercury-cadmium-telluride detector, which is cooled by liquid nitrogen. The entire experimental setup is enclosed to reduce relative humidity fluctuations. A shuttling procedure is used to compensate residual water vapor rotation-vibration bands (15). For this purpose, the home-built trough is divided into two compartments that are connected to ensure the same surface height on both sides. One compartment is monolayer-covered (sample); the other one is monolayer-free (reference). Applying the shuttle mechanism enables the interferograms of sample and reference to be alternately collected. For all measurements at 40 mN/m, *p*-polarized radiation was used at an angle of incidence of 40°.

A total of 400 scans were acquired with a scanner velocity of 20 kHz at a resolution of 8 cm^{-1}. The scans were coadded, apodized with the Blackman-Harris three-term function, and fast Fourier transformed with one level of zero filling to produce spectral data encoded at 4 cm^{-1} intervals. IRRA spectra are presented as absorbance versus wavenumber. Absorbance, also reflectance-absorbance, is obtained from $-\lg(R/R_0)$, where R is the single-beam reflectance of the sample and R_0 the single-beam reflectance of the reference. The spectra were baseline-corrected before peak positions and intensities were determined. Peak heights rather than integrated intensities were used to minimize interference from overlapping spectral features.

X-ray diffraction

Grazing incidence x-ray diffraction experiments were performed at the undulator beamline BW1 at HASYLAB, DESY (Hamburg, Germany) using a liquid-surface diffractometer. A beryllium crystal was employed to obtain monochromatic radiation ($\lambda \cong 1.3$ Å) from the synchrotron source. Concurrently, the beam was deflected downward to strike the monolayer at an angle of incidence $\alpha_i = 0.85\ \alpha_c$, where $\alpha_c \cong 0.13°$ is the critical angle for total external reflection. The intensity of the diffracted beam was detected with a linear position-sensitive detector (OEM-100-M, Braun, Garching, Germany) as a function of the vertical scattering angle α_f. A Soller collimator was located in front of the detector. By rotating this assembly, we could scan the horizontal scattering angle 2Θ. By this means the out-of-plane [$Q_z \cong (2\pi/\lambda)\ \sin\alpha_f$] and the in-plane [$Q_{xy} \cong (4\pi/\lambda)\ \sin(2\Theta/2)$] components of the scattering vector Q were detected simultaneously. Q_{xy} provides information about the laterally periodic structure of the monolayer, whereas Q_z gives information about the tilt angle and the tilt direction of lipid chains. The experimental setup and evaluation procedure have been described in detail elsewhere (16–19).

Brewster angle microscopy

The morphology of the monolayer was imaged with a Brewster angle microscope, model BAM2*plus* from NanoFilm Technologie (Göttingen, Germany), set up above a miniature film balance from NIMA Technology

(Coventry, UK), both mounted on an antivibration table. The microscope was equipped with a frequency-doubled Nd:YAG laser (532 nm; ~50 mW), a polarizer, an analyzer, and a CCD camera. When *p*-polarized light is directed onto the pure air/water interface at the Brewster angle (~53.1°), zero reflectivity is observed. The presence of a monolayer causes light to be reflected, which is then registered by the CCD camera after passing the analyzer. BAM images of 355 × 470 μm^2 were digitally recorded during compression of the monolayer. The lateral resolution was ~2 μm.

Atomic force microscopy

AFM images of the solid-supported monolayers were obtained using a MultiMode scanning probe microscope equipped with a NanoScope IIIa controller (both from Digital Instruments, Santa Barbara, CA) and a 15-μm scanner. Silicon tips (NanoWorld, Neuchâtel, Switzerland) with a resonance frequency of ~285 kHz and a spring constant of ~42 N/m were used for operation in the tapping mode with a scan rate of 0.8 Hz. Only height images are shown here. Samples were prepared by the Langmuir-Blodgett (LB) technique: The compressed monolayers were transferred onto silicon wafers with a pulling rate of ~4 mm/min. During the transfer, the surface pressure was maintained constant with an accuracy of ±0.1 mN/m. Before usage, the silicon wafers were cleaned by the RCA-1 method (20); the resulting oxide layer was not removed.

RESULTS AND DISCUSSION

IRRA spectroscopy

To follow the hydrolysis reaction, the amount of remaining substrate or accumulating product in the monolayer must be determined. IRRAS measurements of mixtures of substrate and product—with and without additive—in the absence of scPLD provide sufficient information to establish a reference system. The calculated calibration curves link the DPPC fraction within the monolayer to the intensity of the asymmetric phosphate stretching vibration $\nu_{as}(PO_2^-)$ of DPPC. The following paragraph describes the main criteria for creating these reference curves.

Fig. 1 *A* shows the IRRA spectra of DPPC, DPPA, and mixtures of the two phospholipids with different molar ratios in a spectral range of 1400–900 cm^{-1}. This region contains different phosphate stretching vibration bands. DPPC generates $\nu_{as}(PO_2^-)$ at 1233 cm^{-1} and $\nu_s(PO_2^-)$ at 1089 cm^{-1}. The intensity of $\nu_{as}(PO_2^-)$ gradually decreases when DPPC is mixed with increasing fractions of DPPA (12,21). For pure DPPA, the phosphate stretching vibrations are caused by two components: PO_2^- and PO_3^{2-}. Both ionization states of DPPA are present at pH 8.0 as the pK_2 of phosphatidic acid is ~8 under conditions corresponding to the buffer used (22,23). Thus, $\nu_{as}(PO_2^-)$ appears at 1167 cm^{-1} and $\nu_{as}(PO_3^{2-})$ at 1100 cm^{-1} (24). Because $\nu_{as}(PO_3^{2-})$ interferes with $\nu_s(PO_2^-)$, the variation of intensity in this frequency range does not correlate with the change in DPPC mole fractions. The vibrations of C-N^+-C at 974 cm^{-1} and R_1O-P-OR_2 at 1061 cm^{-1} are exclusive to DPPC (21,25), but their intensities are comparatively weak. Hence, the only suitable IR band to indicate the amount of DPPC in mixtures with DPPA is $\nu_{as}(PO_2^-)$ at 1233 cm^{-1}.

Fig. 1 *B* shows the mean intensities of this band as a function of the DPPC mole fraction. The data points are fitted linearly to produce a calibration curve with a standard deviation of 1.7×10^{-4}. The linear correlation implies that the molecular orientation of the phosphate group does not affect the $\nu_{as}(PO_2^-)$ intensity. Therefore, solely the amount of DPPC in the monolayer contributes to the intensity of the band. However, if the data point for pure DPPC ($x_{DPPC} = 1$) is excluded from the fitting procedure, the standard deviation of the linear relation is reduced by a factor of 2. In other words, the measured intensity for pure DPPC is ~15 % lower than the value calculated from the calibration curve. The difference is most likely caused by a slight change in the orientation of the phosphate group in pure versus mixed DPPC. This effect does not influence the quantification of DPPC in hydrolysis reactions with high turnover numbers but should be considered

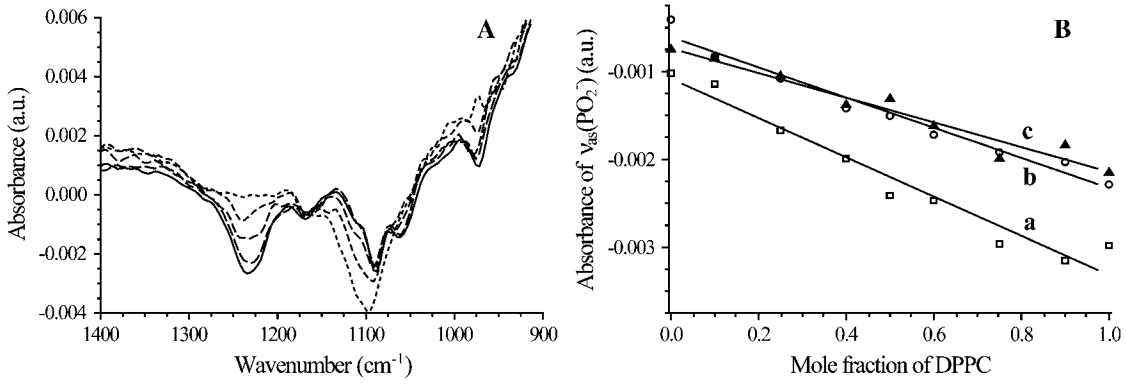

FIGURE 1 (*A*) IRRA spectra of DPPC/DPPA monolayers of different mixing ratios at a surface pressure of 40 mN/m. Representative spectra are shown for (*solid line*) pure DPPC; (*dashed lines, from long to short dashes*) DPPC/DPPA at molar ratios of 75:25, 50:50, and 25:75; and (*dotted line*) pure DPPA on aqueous buffered subphase at 20°C. (*B*) Absorbance of the asymmetric phosphate stretching vibration $\nu_{as}(PO_2^-)$ as a function of the DPPC mole fraction in mixtures with DPPA. Symbols represent mean intensities of $\nu_{as}(PO_2^-)$ in the pure phospholipid system, i.e., (□) DPPC/DPPA only, and in the mixed systems of (○) phospholipids/C_{16}OH and (▲) phospholipids/DPG, respectively, both 1:1 (mol/mol). The indicated mole fraction of DPPC solely considers the DPPC/DPPA ratio in a system. Lines represent the best linear fits for (*a*) DPPC/DPPA, (*b*) DPPC/DPPA/C_{16}OH, and (*c*) DPPC/DPPA/DPG. Because the absorbance of $\nu_{as}(PO_2^-)$ is negative, the most intense band, i.e., $x_{DPPC} = 1$, produces the lowest absorbance value.

when a low or zero conversion rate is observed. The latter two cases are difficult to distinguish because the decrease in $\nu_{as}(PO_2^-)$ intensity on the initial formation of DPPA is possibly compensated by a slight reorientation of the DPPC headgroup.

To obtain calibration curves for the monolayers including $C_{16}OH$ or DPG, the same approach was applied (Fig. 1 *B*). Mean intensities of $\nu_{as}(PO_2^-)$ are taken from IRRA spectra of phospholipid/additive mixtures (1:1, mol/mol), in which the phospholipid moiety consists of DPPC/DPPA at varying molar ratios (spectra not shown). Again, the $\nu_{as}(PO_2^-)$ absorbance of DPPC at ~1230 cm^{-1} continuously diminishes for decreasing amounts of DPPC. A linear fit correlates the intensity of $\nu_{as}(PO_2^-)$ with the mole fraction of DPPC in the phospholipid moiety of the mixed system. Please note that the plot refers to the total phospholipid composition of the mixtures, not considering the additive fraction. Hence, all calibration curves link the DPPC/DPPA ratio to the $\nu_{as}(PO_2^-)$ intensity; but the total content of DPPC in pure phospholipid monolayers is twice the content of DPPC in monolayers comprising one additive. Therefore, the absorbance for $x_{DPPC} = 1$ in the additive-containing monolayers, i.e., DPPC/$C_{16}OH$ and DPPC/DPG, both 1:1 (mol/mol), approximately equals the absorbance for $x_{DPPC} = 0.5$ in the additive-free monolayers, i.e., DPPC/DPPA 1:1 (mol/mol). The *x* axis of the calibration curves is chosen so that conversion rates of the enzymatic reactions in the different monolayer systems can later be easily compared. The use of these reference curves allows the determination of the amount of substrate remaining in the monolayer during and after hydrolysis with an estimated accuracy of ±5%.

Activity measurements

The yield of the enzymatic hydrolysis of DPPC was investigated as a function of the substrate structure by varying surface pressure and additive content of the monolayer (see Wagner and Brezesinski (13) for compression isotherms). The course of a typical hydrolysis experiment is shown in Fig. 2 *A*. Control spectra of the DPPC monolayer are taken before and after the injection of 50 units scPLD at a surface pressure of 40 mN/m. These initial spectra do not exhibit any difference in the phosphate stretching vibration bands. Hence, hydrolysis is not detectable at 40 mN/m. Additionally, we do not observe any indication of the adsorption of scPLD that significantly affects the orientation of the lipid headgroup and consequently the intensity of $\nu_{as}(PO_2^-)$. Therefore, the different control spectra that are collected at 40 mN/m before and after hydrolysis can be used to quantitatively determine the reaction yield (12,21). To allow hydrolysis, the monolayer is expanded to the desired surface pressure, where the course of the enzymatic reaction is observed overnight by regular IRRAS measurements (Fig. 3). The long reaction time guarantees completion of the process at all surface pressures examined. A final control spectrum, which is recorded after recompression of the monolayer to 40 mN/m, reveals that the $\nu_{as}(PO_2^-)$ band is substantially reduced (Fig. 2 *A*). A negative control experiment without scPLD did not result in any significant changes. Thus, the intensity decrease observed in the presence of scPLD is caused by enzymatic hydrolysis. Application of the calibration curves allows the $\nu_{as}(PO_2^-)$ band intensity to be converted into the amount of hydrolyzed substrate.

Fig. 2 *B* depicts the percentage of hydrolyzed substrate as a function of the surface pressure for all three monolayer systems. The pure DPPC monolayer is completely hydrolyzed up to 10 mN/m. An increase of the surface pressure to 20 mN/m slightly reduces the reaction yield to 85%. Above 20 mN/m the hydrolytic turnover drastically decreases until it reaches a value of 18% at 30 mN/m. As explained before, the calibration curves used for the quantification of the

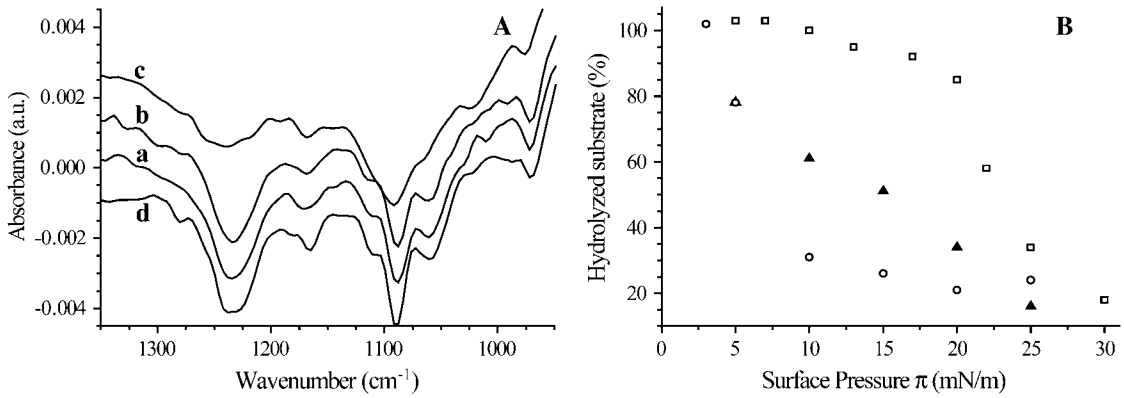

FIGURE 2 (*A*) IRRA spectra of a DPPC monolayer before and after injection of scPLD at a surface pressure of 40 mN/m. Control spectra of the pure DPPC monolayer on aqueous buffered subphase at 20°C were acquired (*a*) before and (*b*) directly after injection of 50 units scPLD. (*c*) Hydrolysis at 20 mN/m had been allowed overnight to ensure completion of the process before a final control spectrum was recorded at 40 mN/m. During the corresponding negative control experiment, the DPPC monolayer was kept at 20 mN/m on a scPLD-free subphase for 20 h. (*d*) Then, an ultimate spectrum was recorded at 40 mN/m. Spectra *b*, *c*, and *d* are shifted for better visualization. (*B*) Amount of hydrolyzed substrate, i.e., DPPC, as a function of the surface pressure of the monolayer during hydrolysis by scPLD. The initial monolayer consisted of (□) pure DPPC and equimolar mixtures of (○) DPPC/$C_{16}OH$ and (▲) DPPC/DPG, respectively.

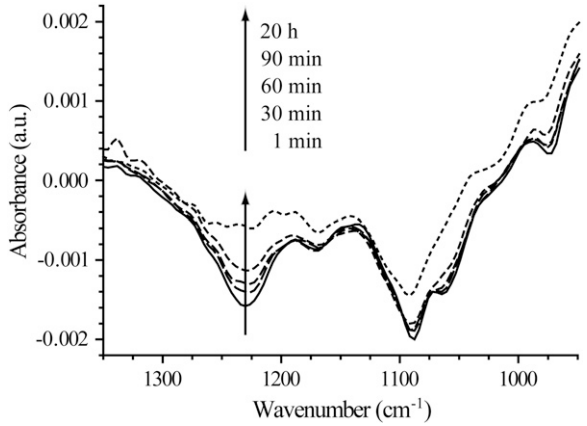

FIGURE 3 Progression of the $\nu_{as}(PO_2^-)$ vibration at 1233 cm^{-1} on hydrolysis of a pure DPPC monolayer at 7 mN/m. After injection of 50 units scPLD, the monolayer was expanded to 7 mN/m, where hydrolysis was observed within the denoted time intervals by acquiring IRRA spectra with *s*-polarized IR light incident at 40°. Residual water vapor rotation-vibrations cause a baseline shift as indicated above 1300 cm^{-1}. Therefore, baseline corrections are referenced to higher wavenumbers, outside the spectral range that is influenced by water vapor absorbance. The spectrum after 20 h corresponds to a complete DPPC turnover. The remaining, wavelike absorptions around 1240 cm^{-1} depict the CH_2 wagging vibrations of the acyl chains.

DPPC/DPPA ratio exhibit larger deviations for pure DPPC (−5% to +20%) than for DPPA-comprising systems (±5%). Hence, a reaction yield of ≤ 20% corresponds to values of $x_{DPPC} \geq 0.8$. Assuming the largest possible error, such reaction yields can equally be interpreted as $x_{DPPC} = 1$, which is equivalent to zero hydrolysis. However, within our measurements it is most likely that tiny amounts of substrate are hydrolyzed in monolayers even at high surface pressure. In conclusion, the graph for the pure phospholipid system displays a sigmoid progression.

A similar decay of the reaction yield is shown for $C_{16}OH$-containing monolayers with increasing surface pressure. The amount of hydrolyzed substrate decreases from 100% at 3 mN/m to ~80% at 5 mN/m and ~30% at 10 mN/m (Fig. 2 *B*). Above 10 mN/m the detected reaction yield remains constant at ~24% and does not diminish to zero up to 25 mN/m. Finally, the addition of DPG to the substrate generates a different progression when the reaction yield is plotted versus the surface pressure of the monolayer (Fig. 2 *B*). The amount of hydrolyzed substrate decreases linearly with rising surface pressure. A linear fit of the data reveals a slope of −3% per 1 mN/m. At 25 mN/m the detected turnover is ~15%.

The linear correlation of reaction yield and surface pressure in the presence of DPG is contrary to the sigmoid progression of the pure and the $C_{16}OH$-comprising substrate films. This difference can have two origins. In a first scenario, the difference is caused by distinct scPLD activities, i.e., direct hydrolysis versus transphosphatidylation followed by hydrolysis, toward the varying substrate systems. The sigmoid curve reflects the enzymatic mechanism that involves immediate hydrolysis of the substrate as observed for a PC monolayer by El Kirat et al. (14). Therefore, DPPC is also directly hydrolyzed in the $C_{16}OH$-containing system. In contrast, the linear dependence between reaction yield and surface pressure in monolayers including DPG could result from another course of the reaction. During the transphosphatidylation, DPG can be used by scPLD for the nucleophilic attack of DPPC. The product is then immediately hydrolyzed to give DPPA and DPG (14). This activating function of DPG could account for the different curve progression as well as the higher reaction yield in the presence of DPG compared to $C_{16}OH$. The precedence of the transphosphatidylation mechanism in presence of DPG but not of $C_{16}OH$ is caused by either a more suitable orientation of the OH-group of DPG within monolayers or a larger molecular area per DPPC headgroup when mixed with DPG (13).

However, it can be equally assumed that the OH-groups of both additives are involved in transphosphatidylation reactions catalyzed by scPLD (14). Therefore, the differing correlations of reaction yield and surface pressure in the two mixed substrate systems must be caused by another process. Within this context, it is necessary to contemplate the activating property of DPG toward the enzyme (26): scPLD was shown to preferentially insert between the acyl chains of DPG (27). Thus, in a second scenario, an enhanced translocation of the enzyme to the DPG-containing monolayer could explain the higher scPLD activity compared to the system including $C_{16}OH$. Moreover, the adsorption of the enzyme to diacylglycerol monolayers is linearly reduced with increasing surface pressure (27). Accordingly, the linear decrease of the reaction yield versus surface pressure in the presence of DPG can be attributed to desorption of the enzyme.

In summary, there are two scenarios that account for the distinct line shapes in the plot of reaction yield versus surface pressure (Fig. 2 *B*). Their consequences for the investigation of the influence of substrate structure on the enzymatic activity are different. In the first case, varying enzymatic mechanisms are assumed; the final products are, however, the same—independent of the course of reaction. Therefore, the proposed systems are appropriate to determine scPLD activity in dependence on the substrate monolayer structure as long as the view is not restricted to the hydrolytic activity. In the second case, a presumably different adsorption behavior of scPLD toward the DPG-including monolayer separates this system from the other two. Hence, the experimental system comprising DPG can only be cautiously compared to pure substrate or $C_{16}OH$-containing monolayers.

Substrate monolayer structure

The activity survey reveals that the critical surface pressure π_c above which scPLD is unable to efficiently convert DPPC is very different for the three systems. The activity toward pure substrate monolayers is suppressed at $\pi_c \geq 30$ mN/m.

In the case of equimolar mixtures of DPPC/C_{16}OH, the enzymatic reaction is distinctly constricted above 10 mN/m. In equimolar DPPC/DPG monolayers, the suppression of scPLD activity occurs at $\pi_c \geq 25$ mN/m. These critical surface pressures can be correlated with specific structural parameters of the monolayer (13): The tilt angle of the hydrophobic chains reflects the lipid packing density, and the area per headgroup signifies the accessibility of the point of attack for the enzyme. To identify the aspect that is essential for scPLD activity, the structures of the different monolayers at π_c need to be compared. Pure DPPC monolayers at π_c exhibit a tilt angle of the acyl chains of ~32° and an area per headgroup of ~48 Å^2 (13). In the presence of C_{16}OH, the corresponding values are ~23° and ~65 Å^2 (i.e., the area of three chains neglecting the volume of the hydroxyl group of C_{16}OH). In the presence of DPG, the acyl chains are untilted at π_c, and the area per DPPC headgroup amounts to ~80 Å^2 (i.e., the area of four chains) (13). Because neither the chain tilt nor the area per DPPC headgroup is constant in the three experimental systems, a structural feature other than the lipid packing density must be crucial for an efficient activity of scPLD. Instead of distinct parameters of the lipid molecule structure, other monolayer characteristics should be decisive for scPLD activation and are identified in the following.

We investigated monolayers of equimolar mixtures of substrate and product, i.e., DPPC/DPPA, with and without additive. X-ray diffraction experiments allow us to distinguish between different condensed structures within one monolayer. A condensed-phase immiscibility is inferred for a mixture of DPPC and DPPA over a wide range of surface pressure from the known phase diagram of the two components (28). Moreover, our data show an immiscibility behavior that is significantly changed on the addition of C_{16}OH or DPG, respectively. These results are discussed in detail on the basis of Fig. 4 and Table 1.

The contour plot of the DPPC/DPPA (1:1, mol/mol) monolayer at 15 mN/m displays four Bragg reflections, which cannot be assigned to a single condensed structure (Fig. 4 *B*): The two peaks at lower Q_{xy} values describe a strongly tilted L_2 phase, whereas the two peaks at higher Q_{xy} depict a less tilted Overbeck phase (Table 1). The phases can be attributed to DPPC- and DPPA-rich domains, respectively (28). With increasing surface pressure, the tilt angle of the acyl chains in both phases reduces, and the DPPA-rich domains adopt a hexagonal structure (Fig. 4 *C*). In contrast, at a lowered surface pressure of 5 mN/m, only one rectangular structure is observed, corresponding to a tilted, DPPA-rich phase (Fig. 4 *A*). DPPC-rich domains cannot be monitored at 5 mN/m, which is close to the transition pressure of pure DPPC, because the domains are still in the liquid-expanded phase state (13). In summary, phase separation occurs in the mixed phospholipid monolayer at all surface pressures.

When the additives C_{16}OH or DPG are included in the equimolar phospholipid mixture, the x-ray diffraction data are considerably changed (Fig. 4, *D–I*): All contour plots exhibit either one, two, or three Bragg reflections that originate from a single condensed structure that is either hexagonal, rectangular, or oblique (Table 1). Two different condensed phases are not detected at the same time in the presence of an additive. Hence, C_{16}OH and DPG appear to mediate the miscibility of DPPC and DPPA in the ternary mixtures.

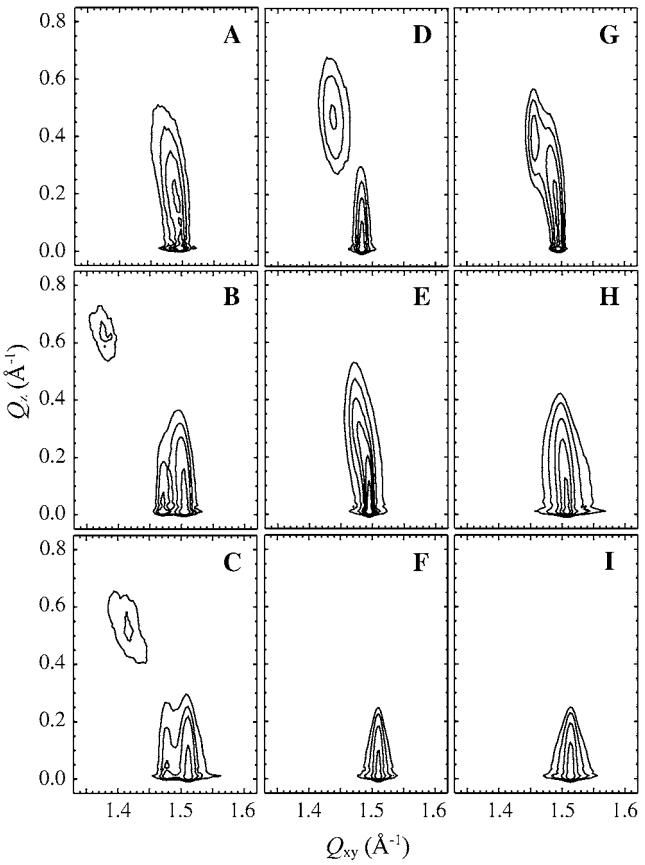

FIGURE 4 Contour plots of the corrected x-ray intensities as a function of the in-plane (Q_{xy}) and out-of-plane (Q_z) components of the scattering vector Q of the following monolayers on aqueous buffered subphase at 20°C: molar mixtures of (*A–C*) DPPC/DPPA 1:1, (*D–F*) DPPC/DPPA/C_{16}OH 1:1:2, and (*G–I*) DPPC/DPPA/DPG 1:1:2 at a surface pressure of (*A*, *D*, and *G*) 5 mN/m, (*B*, *E*, and *H*) 15 mN/m, and (*C*, *F*, and *I*) 25 mN/m.

The lack of phase separation in the additive-containing systems correlates with the observation of a reduced activity of scPLD toward these monolayers. In other words, we assume that phase separation of the reaction product DPPA is crucial for high scPLD activity as seen during the hydrolysis of pure DPPC monolayers. If the generated DPPA is not segregated from the substrate structure, the activity of scPLD will be diminished. In fact, PA aggregation facilitates the formation of a 2:1 PA-Ca^{2+} complex (or vice versa), which is supposed to specifically bind to the allosteric site of scPLD (27). Thus, the enzyme can be activated through different effects: 1), the orientation of the enzyme becomes more suitable to bind a substrate molecule near the domain boundaries; 2), the proteins aggregate after binding to a PA-rich

TABLE 1 Diffraction peak positions, tilt angles *t*, and in-plane areas A_{xy} of an alkyl chain in the indicated monolayers at different surface pressures π on aqueous buffered subphase at 20°C

π (mN/m)	Q_{xy} (Å^{-1})	Q_z (Å^{-1})	t (°)	A_{xy} (Å^2)
DPPC/DPPA (1:1, mol/mol)				
5.2	1.477*	0.303	11.6	20.6
	1.494*	0.152		
14.8	1.498*	0.182	6.9	20.2
	1.504*	0.091		
	1.382†	0.607	27.4	22.9
	1.470†	0.000		
24.8	1.511*	0.000	0.0	20.0
	1.417†	0.546	24.3	22.1
	1.478†	0.000		
DPPC/DPPA/C_{16}OH (1:1:2, mol/mol)				
5.6	1.439	0.470	20.9	21.6
	1.483	0.000		
15.0	1.474	0.336	13.6	20.7
	1.488	0.266		
	1.495	0.070		
24.6	1.510	0	0	20.0
DPPC/DPPA/DPG (1:1:2, mol/mol)				
5.2	1.458	0.369	14.2	20.8
	1.490	0.184		
15.2	1.502	0.178	6.8	20.1
	1.509	0.089		
24.8	1.513	0	0	19.9

The in-plane (Q_{xy}) and out-of-plane (Q_z) components of the scattering vector Q are given by selected best-fit values.
*Refers to DPPA-rich domains.
†Refers to DPPC-rich domains.

domain and are activated by oligomerization (10); 3), the enzyme adopts an active conformation to productively bind the substrate and release PA from the active site (7). The last mechanism prevents a product inhibition of scPLD in the presence of Ca^{2+}.

To validate the concept of product segregation being the decisive prerequisite to scPLD activation, the following aspects of our results must be discussed. Both additives mediate miscibility between lipid substrate and product, but the scPLD activity toward the DPG-comprising system is less reduced than in the C_{16}OH-including monolayer. This difference is possibly related to the activating properties of DPG that have been previously described. Therefore, an enzymatic activity is monitored, although DPG prevents the segregation of DPPA. Consequently, the evaluation of this system is not as straightforward as initially expected, and it should be studied further.

The reaction yield of the C_{16}OH-containing monolayers reaches ~24 % at surface pressures above 10 mN/m. However, a condensed phase separation is not detected for a corresponding mixture comprising 10% DPPA (i.e., DPPC/DPPA/C_{16}OH (9:1:10, mol/mol), data not shown). This apparent discrepancy can have different origins including the problem of lateral resolution of the x-ray technique, but it is most likely caused by a basal activity of scPLD. This basal activity promotes the conversion of a distinct amount of substrate without any specific activation of the enzyme. Once enough PA is formed and phase-separated within the monolayer, the enzyme is activated. This process is described as the lag-burst behavior of scPLD toward pure DPPC monolayers (11,21). If the product of the basal activity is not segregated from the substrate, the enzyme will not be activated. This case is observed for the C_{16}OH-containing system: A sufficient reaction time allows scPLD to convert up to ~24% of the DPPC. Then, the enzymatic activity ceases because the produced DPPA is not phase-separated in the presence of C_{16}OH.

This model raises the question of why scPLD is highly active toward monolayers including C_{16}OH at surface pressures below 10 mN/m. Again, a condensed phase separation of the product is not detected by x-ray diffraction (Fig. 4 *D*). However, the existence of a second liquid-expanded phase (L) cannot be precluded at this low surface pressure. We therefore investigated the molar mixtures of DPPC/DPPA/C_{16}OH (1:1:2) by techniques that are able to show L/C phase coexistence.

BAM images of the mixed monolayer reveal morphological characteristics in the micrometer range at different compression states (Fig. 5). Coexisting dark and bright regions are observed at very low surface pressure near the lift-off point of the isotherm (Fig. 5 *A*). The irregular shape of the darker domains indicates that they correspond to the gas phase of the monolayer. The brighter zones reflect a condensed phase state, which persists up to high surface pressures. In addition, few bright spots can be seen, which do not grow on monolayer compression and are attributable to the nucleation of DPPA forming small, three-dimensional structures (29). On increasing surface pressure, the gas phase disappears, and only few defects are observed within the condensed monolayer at 3 mN/m (Fig. 5 *B*). At 5 mN/m, the film appears in a single phase state (Fig. 5 *C*). A transition involving the liquid-expanded phase is not detected by BAM with a lateral resolution of ~2 μm.

To resolve structures on a size scale that is much closer to the diameter of the enzyme, AFM measurements of LB transfers were performed. This technique provides images of the mixed monolayer of DPPC/DPPA/C_{16}OH (1:1:2, mol/mol) with a lateral resolution in the nanometer range. Fig. 5 *D* shows the film at 3 mN/m, where it widely exhibits a condensed phase state (cf. BAM results). Oval domains with a constant width of ~450 nm are ~3–6 Å lower in height than the surrounding condensed regions. This height difference is consistent with values reported for the change from L to C phase (30). Hence, the observed domains contain molecules in the liquid-expanded phase state, which could not be observed by BAM because of their small size. The elongated shape of these domains is most likely caused by a draining of the subphase during transfer. Small circular holes ~60 nm in

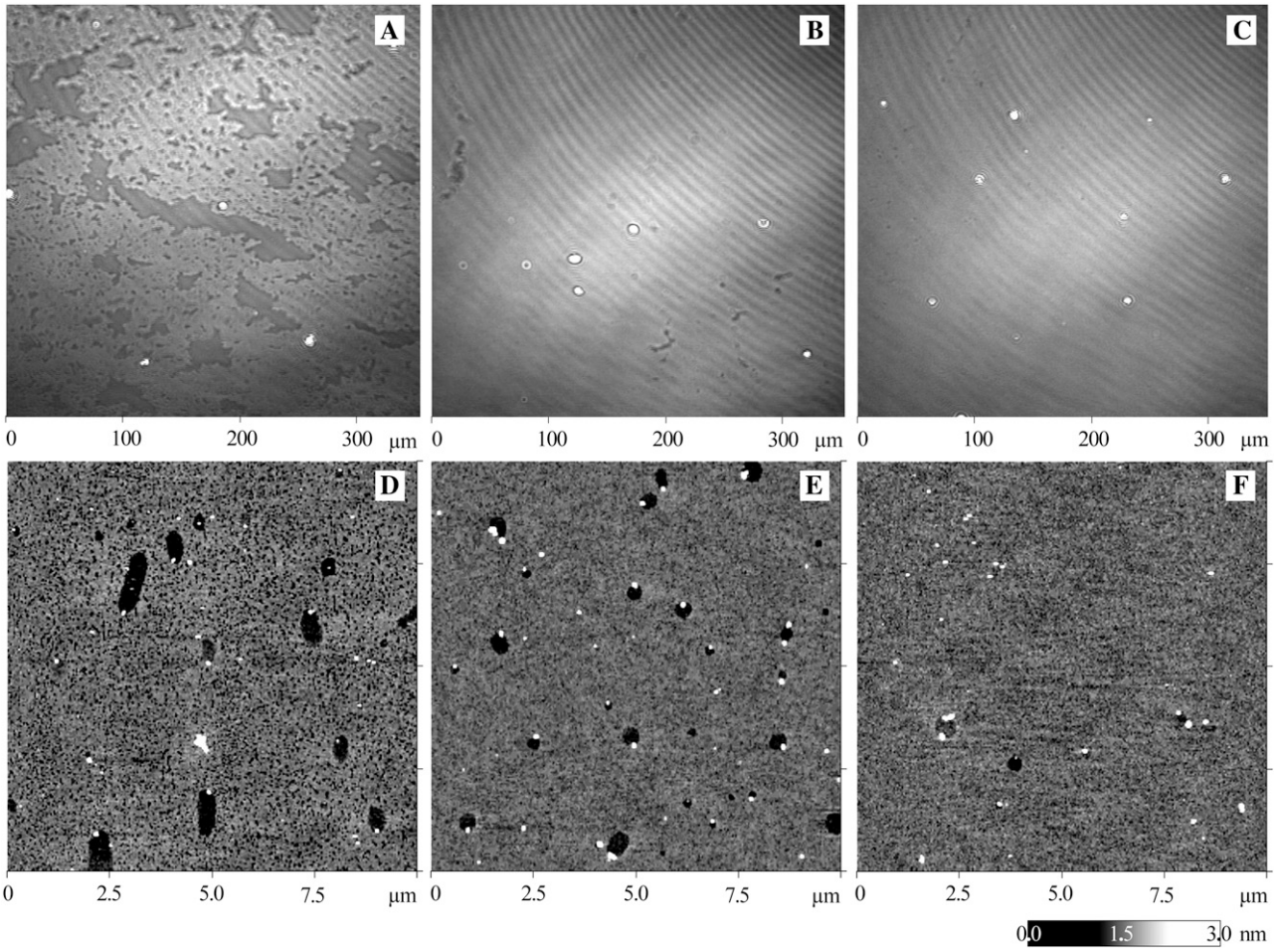

FIGURE 5 Morphology of the mixed monolayer of DPPC/DPPA/C_{16}OH 1:1:2 at different surface pressures. (*First row*) BAM images of the monolayer on aqueous buffered subphase at 20°C recorded at (*A*) 0.2 mN/m, (*B*) 3.1 mN/m, and (*C*) 5.0 mN/m. The image size is 355 × 355 μm^2. (*Second row*) AFM images of the monolayer transferred onto silicon wafers at (*D*) 3.0 mN/m, (*E*) 5.0 mN/m, and (*F*) 7.0 mN/m. The image size is 10 × 10 μm^2. The relatively high surface roughness in the AFM pictures is caused by the oxide layer on the silicon wafers, which was not removed after RCA-1 cleaning (38). The white points of increased height represent aggregates on the monolayer.

diameter and ~1 nm in depth are also generated during the transfer onto the solid support. The latter is known to cause a further condensation of the monolayer (31). Because the molecules are too rigid to respond to this condensation, the process is frequently interrupted during transfer, and pinholes are formed.

At 5 mN/m, the molecules in the condensed phase are more tightly packed than at 3 mN/m; so the monolayer becomes less sensitive to the additional condensing effect of the silicon wafer (Fig. 5 *E*). The film exhibits fewer and also smaller pinholes. Because the whole monolayer is more rigid, the liquid-expanded domains are hardly elongated, but rather round with a diameter of ~400 nm. Increasing the surface pressure to 7 mN/m leads to a strong diminution of the liquid-expanded phase (Fig. 5 *F*). At 10 mN/m, the film is completely homogeneous (data not shown). It is concluded that an L/C phase separation does not occur at surface pressures above 7 mN/m.

The transition point from a phase-separated to a homogeneous monolayer at 7 mN/m for 50% DPPA (i.e., hydrolyzed substrate) coincides with the critical surface pressure π_c above which scPLD is unable to efficiently convert DPPC in a C_{16}OH-comprising system (cf. Fig. 2 *B*). This result confirms the necessity of phase separation for high scPLD activity. From our point of view, this study of the substrate monolayer structure provides the first direct proof for what has previously been anticipated (9,11,12): The segregation of the reaction product PA is essential for the activation of scPLD. The different possibilities of activating mechanisms have been discussed earlier in this article.

Product monolayer structure

Regarding the hydrolysis of pure DPPC monolayers at higher surface pressure, it becomes evident that there is a limitation of the activation of scPLD through the segregation

of DPPA. Above 20 mN/m, the hydrolytic turnover drastically decreases, although the system shows phase separation of substrate- and product-rich domains, respectively (cf. Figs. 2 *B* and 4 *C*). A comparison of the amount of hydrolyzed substrate to the phase diagram of DPPC and DPPA on a similar buffer system (28) reveals an interesting correlation (see Fig. 7): Up to 20 mN/m, the maximum turnover concurs with the transition of the DPPA-rich phase from a tilted to an untilted structure. However, above 20 mN/m, the maximum turnover does not correspond to the hypothesized transition line.

Therefore, we verified the structural transitions of the DPPA-rich domains within mixed monolayers of DPPC/DPPA at different molar mixing ratios by x-ray diffraction. The results show that the DPPA-rich phase initially forms a rectangular structure within all tested mixtures (Table 1 includes some of the data). The corresponding tilt angle of the acyl chains t reduces with increasing surface pressure until the hexagonal phase state is reached. A plot of 1/cos t as a function of π (Fig. 6) allows us to determine the surface pressure π_t at which the tilted molecules change their orientation to upright (13). Extrapolation of the plot to zero tilt (1/cos $t = 1$) provides the following values: $\pi_t = 25.1$ mN/m for 7:3 (mol/mol), $\pi_t = 22.1$ mN/m for 1:1 (mol/mol), and $\pi_t = 19.8$ mN/m for 3:7 (mol/mol) mixtures of DPPC/DPPA. These points are added to the known phase diagram (Fig. 7) and replace the dotted line, which was originally hypothesized by Estrela-Lopis et al. (28). The observed deviation is most probably caused by the reduced Ca^{2+} concentration of 120 μM used in the present buffer system. The authors of the original phase diagram used a subphase containing 50 mM $CaCl_2$, which promotes the condensation of DPPA (32,33) and generates an untilted structure at slightly lower surface pressures.

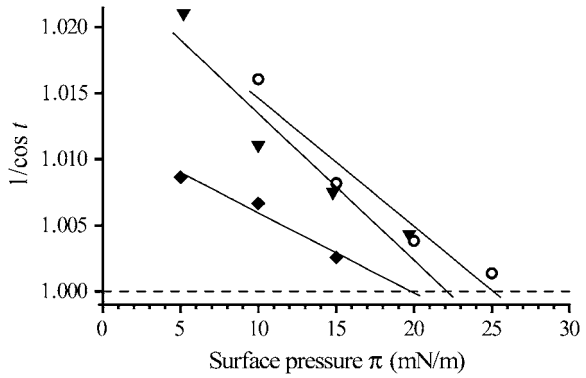

FIGURE 6 Dependence of the tilt angle t on the surface pressure π in mixed monolayers of DPPC/DPPA at molar mixing ratios of (○) 7:3, (▼) 1:1, and (♦) 3:7 on aqueous buffered subphase at 20°C. Values of 1/cos t are plotted as a function of π. Lines represent best linear fits. Extrapolation of the plot to zero tilt (1/cos $t = 1$) is defined as the pressure π_t, at which the tilted molecules change their orientation to upright.

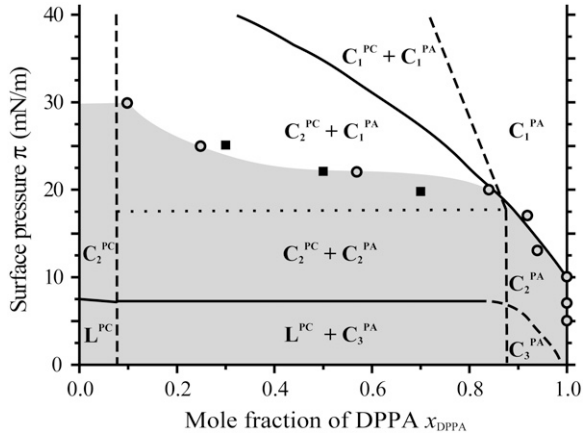

FIGURE 7 Surface pressure dependence of the phase behavior of DPPC/DPPA monolayers and of the turnover rate of scPLD at 20°C. The phase diagram is adapted from Estrela-Lopis et al. (28) and depicts liquid-expanded (L), oblique (C_3), rectangular (C_2), and hexagonal (C_1) phase states of DPPC- (superscript PC) and DPPA (superscript PA)-rich phases. Solid lines indicate experimentally observed phase transitions; dashed and dotted lines represent approximated phase boundaries. The transition pressures π_t (■), which are determined for the different mixed monolayers on a buffered subphase containing 120 μM $CaCl_2$ (cf. Fig. 6), replace the dotted line according to Estrela-Lopis et al. (28), where the buffered subphase contained 50 mM $CaCl_2$. The maximum enzymatic turnover at each surface pressure (○) limits the range of monolayer phase states where scPLD activity is observed (*shaded in gray*).

The corrected transition pressures in the phase diagram agree with the maximum turnover of DPPC above 20 mN/m within the error range. Hence, no hydrolysis can be observed when the reaction product DPPA adopts an untilted phase state. We therefore postulate that a hexagonal structure within the PA-rich domains inhibits scPLD activity.

CONCLUSION

Previously, PLD from *Streptomyces chromofuscus* was shown to efficiently hydrolyze DMPC monolayers at 30 mN/m (11). This surface pressure is widely assumed to be physiologically relevant (34). Our study aimed at examining the influence of membrane structure on the catalytic activity of scPLD. Three analogous substrate-containing monolayer systems were utilized because they provide different phase structures at similar surface pressures. The results presented reveal that the activity of scPLD depends neither on a particular surface pressure nor on conformational features of the lipid substrate as assumed before (12,21). Instead, the enzymatic activity correlates with distinct phase states of the model membranes used.

Earlier investigations have suggested that the lag-burst behavior of the enzyme is associated with a lateral segregation of the reaction product PA (9,11,12). Here we prove that high scPLD activity requires the phase separation of PA. The corresponding mechanism of scPLD activation is illustrated

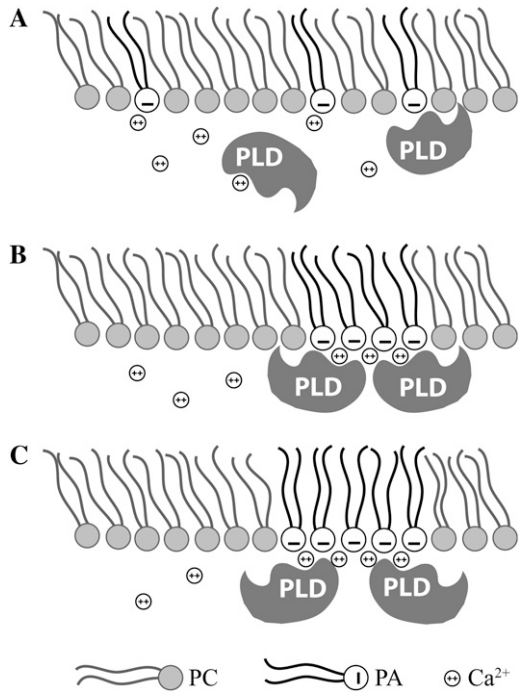

FIGURE 8 Model of the regulation of scPLD. (*A*) Basal activity of scPLD toward monolayers of PC. The enzymatic conversion of PC to PA requires the presence of Ca^{2+}. (*B*) Activation of scPLD. (*C*) Inhibition of scPLD.

in Fig. 8, *A* and *B*. Once a critical amount of PC is converted into PA by the basal activity of the enzyme, the product becomes immiscible with the substrate and segregates into PA-rich domains. These domains enable the formation 2:1 PA/Ca^{2+} complexes (or vice versa) that are hypothesized to preferentially interact with the enzyme (27). Thus, product segregation activates scPLD. In addition, the enzyme can be inhibited through PA-rich domains adopting a hexagonal structure (Fig. 8 *C*). This phase state is characterized by the upright alignment of the lipid chains. These untilted chains indicate a changed orientation of the PA headgroup that complementarily affects the orientation of bound enzyme. Hence, scPLD is impeded to continue the hydrolysis of PC neighboring the PA-rich domains.

Such a scenario for enzyme inhibition is also conceivable in biological membranes on local changes in composition and/or surface pressure of this highly dynamic system (35,36). More ordered lipid structures are found in cell membranes, e.g., in cholesterol-rich domains and in the vicinity of transmembrane proteins. Fluctuations of the surface pressure can occur in a range of 3 and 10 mN/m without membrane disruption (37) and might thus lead to the kinds of local changes in the phase state of the membrane that are crucial for scPLD activation and inhibition. In summary, the obtained results introduce compelling evidence for how membrane structure regulates the activity of lipid-modifying enzymes and therefore the concentration of lipid messengers such as PA.

The authors would like to thank HASYLAB at DESY (Hamburg, Germany) for beam time at BW1, Anne Heilig for AFM measurements, and Annabel Muenter for proofreading the manuscript.

REFERENCES

1. Cazzolli, R., A. N. Shemon, M. Q. Fang, and W. E. Hughes. 2006. Phospholipid signalling through phospholipase D and phosphatidic acid. *IUBMB Life*. 58:457–461.
2. Jenkins, G. M., and M. A. Frohman. 2005. Phospholipase D: a lipid centric review. *Cell. Mol. Life Sci.* 62:2305–2316.
3. Liscovitch, M., M. Czarny, G. Fiucci, and X. Q. Tang. 2000. Phospholipase D: molecular and cell biology of a novel gene family. *Biochem. J.* 345:401–415.
4. Yang, H. Y., and M. F. Roberts. 2002. Cloning, overexpression, and characterization of a bacterial Ca^{2+}-dependent phospholipase D. *Protein Sci.* 11:2958–2968.
5. Zambonelli, C., and M. F. Roberts. 2005. Non-HKD phospholipase D enzymes: new players in phosphatidic acid signaling? *In* Progress in Nucleic Acid Research and Molecular Biology, Vol. 79. K. Moldave, editor. Elsevier Academic Press, Amsterdam. 133–181.
6. Geng, D., D. P. Baker, S. F. Foley, C. Zhou, K. Stieglitz, and M. F. Roberts. 1999. A 20-kDa domain is required for phosphatidic acid-induced allosteric activation of phospholipase D from *Streptomyces chromofuscus*. *Biochim. Biophys. Acta.* 1430:234–244.
7. Yang, H. Y., and M. F. Roberts. 2003. Phosphohydrolase and transphosphatidylation reactions of two *Streptomyces* phospholipase D enzymes: covalent versus noncovalent catalysis. *Protein Sci.* 12:2087–2098.
8. Zambonelli, C., and M. F. Roberts. 2003. An iron-dependent bacterial phospholipase D reminiscent of purple acid phosphatases. *J. Biol. Chem.* 278:13706–13711.
9. Geng, D., J. Chura, and M. F. Roberts. 1998. Activation of phospholipase D by phosphatidic acid- enhanced vesicle binding, phosphatidic acid Ca^{2+} interaction, or an allosteric effect? *J. Biol. Chem.* 273:12195–12202.
10. Stieglitz, K., B. Seaton, and M. F. Roberts. 1999. The role of interfacial binding in the activation of *Streptomyces chromofuscus* phospholipase D by phosphatidic acid. *J. Biol. Chem.* 274:35367–35374.
11. El Kirat, K., F. Besson, A. F. Prigent, J. P. Chauvet, and B. Roux. 2002. Role of calcium and membrane organization on phospholipase D localization and activity—competition between a soluble and an insoluble substrate. *J. Biol. Chem.* 277:21231–21236.
12. Estrela-Lopis, I., G. Brezesinski, and H. Möhwald. 2000. Influence of model membrane structure on phospholipase D activity. *Phys. Chem. Chem. Phys.* 2:4600–4604.
13. Wagner, K., and G. Brezesinski. 2007. Modifying dipalmitoylphosphatidylcholine monolayers by *n*-hexadecanol and dipalmitoylglycerol. *Chem. Phys. Lipids.* 145:119–127.
14. El Kirat, K., A. F. Prigent, J. P. Chauvet, B. Roux, and F. Besson. 2003. Transphosphatidylation activity of *Streptomyces chromofuscus* phospholipase D in biomimetic membranes. *Eur. J. Biochem.* 270: 4523–4530.
15. Flach, C. R., J. W. Brauner, J. W. Taylor, R. C. Baldwin, and R. Mendelsohn. 1994. External reflection FTIR of peptide monolayer films in-situ at the air/water interface—experimental-design, spectra-structure correlations, and effects of hydrogen-deuterium exchange. *Biophys. J.* 67:402–410.
16. Jensen, T. R., and K. Kjaer. 2001. Structural properties and interactions of thin films at the air-liquid interface explored by synchrotron x-ray radiation. *In* Novel Methods to Study Interfacial Layers. D. Möbius, and R. Miller, editors. Elsevier Science B.V., Amsterdam. 205–254.
17. Als-Nielsen, J., D. Jacquemain, K. Kjaer, F. Leveiller, M. Lahav, and L. Leiserowitz. 1994. Principles and applications of grazing-incidence x-ray and neutron-scattering from ordered molecular monolayers at the air-water-interface. *Phys. Rep. Rev. Sec. Phys. Lett.* 246:252–313.

18. Kjaer, K. 1994. Some simple ideas on x-ray reflection and grazing-incidence diffraction from thin surfactant films. *Physica B (Amsterdam).* 198:100–109.

19. Tanaka, M., M. F. Schneider, and G. Brezesinski. 2003. In-plane structures of synthetic oligolactose lipid monolayers—impact of saccharide chain length. *ChemPhysChem.* 4:1316–1322.

20. Kern, W., and D. A. Puotinen. 1970. Cleaning solutions based on hydrogen peroxide for use in silicon semiconductor technology. *RCA Rev.* 31:187–206.

21. Estrela-Lopis, I., G. Brezesinski, and H. Möhwald. 2001. Dipalmitoylphosphatidylcholine/phospholipase D interactions investigated with polarization-modulated infrared reflection absorption spectroscopy. *Biophys. J.* 80:749–754.

22. Tatulian, S. A. 1993. Ionization and ion binding. *In* Phospholipid Handbook. G. Cevc, editor. Marcel Dekker, New York. 511–552.

23. Träuble, H., and H. Eibl. 1974. Electrostatic effects on lipid phase-transitions—membrane structure and ionic environment. *Proc. Natl. Acad. Sci. USA.* 71:214–219.

24. Laroche, G., E. J. Dufourc, J. Dufourcq, and M. Pezolet. 1991. Structure and dynamics of dimyristoylphosphatidic acid calcium complexes by H-2 NMR, infrared, and Raman spectroscopies and small-angle x-ray-diffraction. *Biochemistry.* 30:3105–3114.

25. Arrondo, J. L. R., F. M. Goni, and J. M. Macarulla. 1984. Infrared-spectroscopy of phosphatidylcholines in aqueous suspension—a study of the phosphate group vibrations. *Biochim. Biophys. Acta.* 794:165–168.

26. Yamamoto, I., T. Mazumi, T. Handa, and K. Miyajima. 1993. Effects of 1,2-diacylglycerol and cholesterol on the hydrolysis activity of phospholipase-D in egg-yolk phosphatidylcholine bilayers. *Biochim. Biophys. Acta.* 1145:293–297.

27. El Kirat, K., J. P. Chauvet, B. Roux, and F. Besson. 2004. Streptomyces chromofuscus phospholipase D interaction with lipidic activators at the air-water interface. *Biochim. Biophys. Acta.* 1661:144–153.

28. Estrela-Lopis, I., G. Brezesinski, and H. Möhwald. 2004. Miscibility of DPPC and DPPA in monolayers at the air/water interface. *Chem. Phys. Lipids.* 131:71–80.

29. Minones, J., J. M. R. Patino, J. Minones, P. Dynarowicz-Latka, and C. Carrera. 2002. Structural and topographical characteristics of dipalmitoyl phosphatidic acid in Langmuir monolayers. *J. Colloid Interface Sci.* 249:388–397.

30. Hollars, C. W., and R. C. Dunn. 1998. Submicron structure in L-alpha-dipalmitoylphosphatidylcholine monolayers and bilayers probed with confocal, atomic force, and near-field microscopy. *Biophys. J.* 75: 342–353.

31. Leporatti, S., G. Brezesinski, and H. Möhwald. 2000. Coexistence of phases in monolayers of branched-chain phospholipids investigated by scanning force microscopy. *Colloid Surf. A—Physicochem. Eng. Asp.* 161:159–171.

32. Garidel, P., and A. Blume. 2000. Calcium induced nonideal mixing in liquid-crystalline phosphatidylcholine-phosphatidic acid bilayer membranes. *Langmuir.* 16:1662–1667.

33. Ziegler, W., and A. Blume. 1995. Acyl-chain conformational ordering of individual components in liquid-crystalline bilayers of mixtures of phosphatidylcholines and phosphatidic acids—a comparative FTIR and H-2 NMR-study. *Spectrochim. Acta Part A Mol. Biomol. Spectr.* 51: 1763–1778.

34. Brockman, H. 1999. Lipid monolayers: why use half a membrane to characterize protein-membrane interactions? *Curr. Opin. Struct. Biol.* 9:438–443.

35. Janmey, P. A., and P. K. J. Kinnunen. 2006. Biophysical properties of lipids and dynamic membranes. *Trends Cell Biol.* 16:538–546.

36. McIntosh, T. J., and S. A. Simon. 2006. Roles of bilayer material properties in function and distribution of membrane proteins. *Annu. Rev. Biophys. Biomol. Struct.* 35:177–198.

37. Olbrich, K., W. Rawicz, D. Needham, and E. Evans. 2000. Water permeability and mechanical strength of polyunsaturated lipid bilayers. *Biophys. J.* 79:321–327.

38. Seu, K. J., A. P. Pandey, F. Haque, E. A. Proctor, A. E. Ribbe, and J. S. Hovis. 2007. Effect of surface treatment on diffusion and domain formation in supported lipid bilayers. *Biophys. J.* 92:2445–2450.